Revisiting the quasi-steady state approximation for modeling heat transport during directional crystal growth. The growth rate can and should be calculated!

ARTICLE *in* JOURNAL OF CRYSTAL GROWTH · JUNE 2003

Impact Factor: 1.7 · DOI: 10.1016/S0022-0248(03)01154-0

2 AUTHORS:

Alexander Virozub
Technion - Israel Institute of Technology
12 PUBLICATIONS **123** CITATIONS
SEE PROFILE

Simon Brandon
Technion - Israel Institute of Technology
27 PUBLICATIONS **369** CITATIONS
SEE PROFILE

Available online at www.sciencedirect.com
SCIENCE DIRECT®
Journal of Crystal Growth 254 (2003) 267–278
JOURNAL OF CRYSTAL GROWTH
www.elsevier.com/locate/jcrysgro

Revisiting the quasi-steady state approximation for modeling heat transport during directional crystal growth. The growth rate can and should be calculated!

Alexander Virozub, Simon Brandon*

Department of Chemical Engineering, Technion–Israel Institute of Technology, 32000 Haifa, Israel

Received 20 October 2002; accepted 19 March 2003
Communicated by G.B. McFadden

Abstract

It is often feasible to use a quasi-steady-state (QSS) approach when analyzing heat transport in directional crystal growth systems. In such cases, it is common practice to approximate the growth velocity to be equal to the pull rate (the *induced* growth rate). The a priori unknown growth rate is needed for calculation of the rate of latent heat release during solidification. In this manuscript we propose and demonstrate the use of a modified QSS (MQSS) approach which allows for QSS analysis while taking into account, in a self-consistent manner, the calculated growth rate. The new method is shown to yield (for the model vertical gradient freeze system studied here) results which are in excellent agreement with those obtained from a fully transient model. This is achieved for all system parameter values considered in this manuscript, including those for which the standard QSS (SQSS) approach fails due to large deviations between the induced growth rate (the pull rate) and the actual, calculated growth rate. As expected, the SQSS approach is shown to yield satisfactory results when latent heat release is unimportant as well as in situations where the calculated growth rate is similar in value to the pull rate.

Keywords: A1. Finite element method; A1. Modeling; A1. Quasi-steady state; A2. Directional growth

1. Introduction

When analyzing heat transport during bulk crystal growth, the process is often treated as quasi-steady state (QSS) or as a sequence of quasi-steady states (see Ref. [1] and references within). Even when transient analyses are necessary it is sometimes advisable to perform preliminary QSS calculations (e.g. to determine realistic values of material parameters [1]).

The QSS approach is justified if the characteristic time of the growth process τ_g is much larger than the characteristic time for heat transport τ_t (i.e. $\tau_g/\tau_t \gg 1$). For the case of a heat-conduction-dominated vertical gradient freeze (VGF) slab-shaped system with an assumed uniform furnace temperature gradient throughout the furnace (such a system is presented in detail in Section 2.1) an

*Corresponding author. Tel.: +972-4-8292822; Fax: +972-4-8295672.
E-mail address: cersbsb@tx.technion.ac.il (S. Brandon).

0022-0248/03/$ - see front matter
doi:10.1016/S0022-0248(03)01154-0

estimate of the ratio of these time scales is given by $\tau_g/\tau_t = \alpha L/(V_p B^2)$. Here L, B, α and V_p are the ampoule length (height), ampoule width, the minimum between melt and solid thermal diffusivities, and pull rate[1] (i.e. *induced* growth rate), respectively. Note that non-conductive modes of heat transport may introduce additional time scales which must be accounted for (when relevant) since they may affect the validity of the QSS assumption.

Applying the QSS approximation in crystal growth modeling is considered a well established and straightforward undertaking. However, difficulties associated with the determination of the crystal growth rate (V_g) are typically overlooked. This parameter, which is required when the latent heat of fusion significantly impacts heat transport, is not known a priori. The standard choice for the growth rate involves the assumption that it is equal in magnitude to the system's pull rate. Unfortunately this assumption, referred to in this manuscript as the standard QSS (SQSS) approximation, is not always justified.

The deviation between crystal growth rate and the pull rate, under QSS operating conditions, is well recognized in the literature. Sukanek, in his analytical studies of Bridgman–Stockbarger growth [2,3], confirmed previous experimental [4] and numerical [5] observations of this phenomenon and derived, under certain conditions, a criterion for which the deviations between the velocities is less than 10% in magnitude in over 70% of the ampoule. Derby and Brown, in a detailed analysis of the validity of using the QSS approach when modeling Czochralski growth [6], mentioned that the assumption $V_g = V_p$ can itself lead to significant error even if the above time scales condition is obeyed; in the case of Czochralski growth, however, the mismatch between V_p and V_g is often due to the reduction in melt volume during growth and can therefore be estimated a priori. Finally, it is reasonable to assume that when significant changes take place in the geometric and/or thermal environment of the melt/crystal interface, deviations between V_p and V_g may occur. For example, this is possibly important in confined-growth systems when the melt/crystal interface passes through a cone-shaped region of the ampoule (see e.g. Ref. [7]). A similar effect may occur due to long range radiative heating (or cooling) within a semi-transparent or transparent crystal (as in Ref. [8]) which could continuously change the thermal environment of the interface.

In this contribution we show that it is not necessary to adhere to the often erroneous assumption, associated with the SQSS method, that $V_g = V_p$. Instead we propose a modified QSS (MQSS) approach in which the thermal field, interface shape and position and growth rate are all calculated simultaneously in a self-consistent manner.

2. Model formulation and numerical approach

We present a modified QSS (MQSS) method for crystal growth modeling based on simultaneous calculations of temperature field, melt/crystal interface shape and position as well as the distribution of crystal growth velocity along the interface. Our analysis is restricted to a situation in which heat transport within the crystal and melt is dominated by heat conduction.

2.1. Two-dimensional analysis

The model VGF system (see Fig. 1), whose geometry and dimensions are loosely based on the systems discussed in Refs. [9,10], respectively, involves a vanishingly thin-walled 2-D translationally symmetric slab-shaped ampoule with a width of B and height of L (i.e. $-B/2 < x < B/2$, $0 < y < L$ where x and y are spatial coordinates spanning the horizontal and vertical directions, respectively). The ampoule contains a solid phase ($0 < y < H(x,t)$) and slowly solidifying melt phase ($H(x,t) < y < L$) where $H(x,t)$ is the vertical position of the melt/crystal interface. External ampoule surfaces exchange heat with the furnace walls, which are represented by a uniform vertical (in the y-direction) furnace temperature gradient

[1] For the VGF method the pull rate may be conventionally calculated as $G^\star/G$, where $G^\star$ and G are the furnace cooling rate and furnace temperature gradient, respectively.

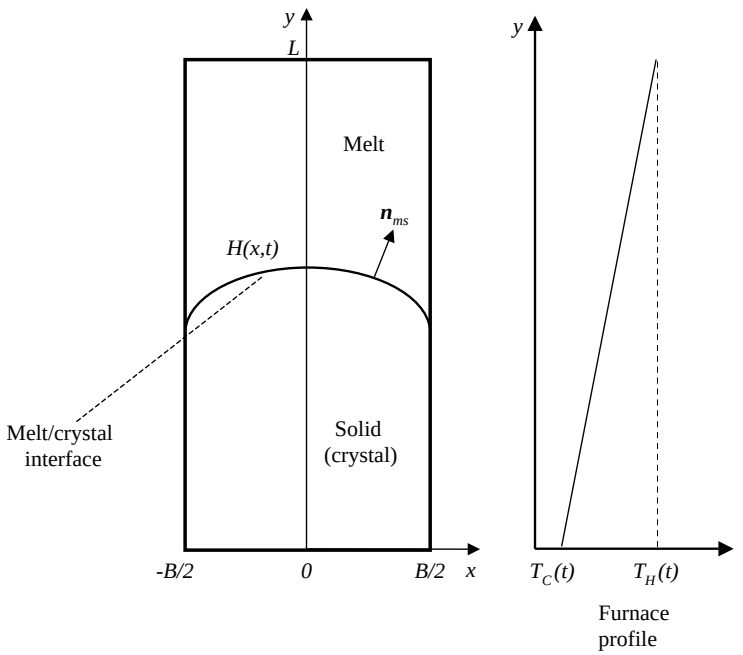

Fig. 1. Mathematical representation of the system and corresponding plot of furnace temperature profile.

G; growth is induced by the reduction of furnace temperatures while keeping G constant. The simplicity of the system studied here is motivated by our interest in discussing issues directly related to the new approach and its validity without being side-tracked by lengthy discussions related to different types of transport phenomena. Initial results for a system involving melt flow and internal radiative transport [11] suggest that extending the MQSS approach to systems with additional transport mechanisms should be straightforward.

The temperature distribution in the melt ($i = \mathrm{m}$) and solid ($i = \mathrm{s}$) is governed by the heat equation:

$$\rho_i C_{p_i} \frac{\partial T}{\partial t} = \nabla \cdot k_i \nabla T, \quad i = \mathrm{m},\ \mathrm{s}, \tag{1}$$

where k_i, ρ_i and C_{p_i} are the thermal conductivity, density and specific heat in the relevant domain, respectively, ∇ is the gradient operator and t denotes time. External boundaries exchange heat by convective transfer with an idealized furnace temperature gradient according to

$$-k_i \nabla T \cdot \mathbf{n} = h(T - T_\mathrm{f}), \quad i = \mathrm{m},\ \mathrm{s}, \tag{2}$$

where $\mathbf{n}$ is the unit normal vector along the boundaries, pointing away from the system, and h is the convective heat transfer coefficient. The furnace temperature, T_f, is given by

$$T_\mathrm{f}(y,t) = T_{\mathrm{C}_0} + Gy - G^\bigstar t, \tag{3}$$

where $T_{\mathrm{C}_0} \equiv T_\mathrm{f}(0,0) = T_\mathrm{mp}$ is the initial temperature at the cold end of the furnace ($y = 0$), while G and $G^\bigstar$ are the (time-independent) furnace temperature gradient and cooling rate, respectively; notice that $t = 0$ is defined as the time when the cold end of the furnace is at the melting point temperature of the solidifying material (T_mp). The time-dependent cold zone and hot-zone temperatures, corresponding to the cold end ($y = 0$) and hot end ($y = L$) of the furnace are given by

$$T_\mathrm{C}(t) = T_\mathrm{f}(0,t) = T_{\mathrm{C}_0} - G^\bigstar t \tag{4}$$

and

$$T_\mathrm{H}(t) = T_\mathrm{f}(L,t) = T_{\mathrm{C}_0} + GL - G^\bigstar t = T_{\mathrm{H}_0} - G^\bigstar t, \tag{5}$$

respectively, where $T_{\mathrm{H}_0} \equiv T_\mathrm{f}(L,0) = T_{\mathrm{C}_0} + GL$ is the initial temperature at the hot end of the furnace ($y = L$). Note that ampoule side walls for

which $x = B/2, 0 < y < L$ or $x = -B/2, 0 < y < L$, exchange heat with T_f given by Eq. (3), while the bottom and top walls for which $y = 0, -B/2 < x < B/2$ and $y = L, -B/2 < x < B/2$, respectively, exchange heat with T_f given by Eqs. (4) and (5), respectively.

Along the melt/crystal interface two conditions must be satisfied: the Stephan condition,

$$[(-k_m \nabla T)_m + (k_s \nabla T)_s] \cdot \mathbf{n}_{ms} = \Delta H_f V_n, \tag{6}$$

and isotherm condition,

$$T = T_{mp}, \tag{7}$$

where ΔH_f is the latent heat of fusion per unit volume of crystalline material, T_{mp} is the melting point temperature of the solidifying material, V_n is the growth velocity in the direction normal to the interface,

$$V_n = V_g(\mathbf{n}_{ms} \cdot \mathbf{e}_y), \tag{8}$$

and $\mathbf{e}_y$ is a unit vector in the y-coordinate direction.

The MQSS method we propose involves the simultaneous solution of two QSS problems for two close instants of time, coupled through an equation which numerically approximates the unknown crystal growth rate V_g. The two problems are both described by the same QSS equations which include the steady-state equation of heat transport in the liquid and solid phases,

$$\nabla \cdot k_i \nabla T = 0, \quad i = m, s, \tag{9}$$

along with the boundary condition given by Eq. (2) and melt/crystal interface conditions described by Eqs. (6) and (7). The small difference in process times associated with the two problems is introduced through Eq. (2) in which T_f depends on time via Eq. (3). Thus two closely related quasi-steady temperature fields $T^{(1)}(x, y)$ and $T^{(2)}(x, y)$, each spanning both the melt and the solid domains, are simultaneously calculated by introducing, in Eq. (3), the two time values $t^{(1)}$ and $t^{(2)} = t^{(1)} + \Delta t$, respectively.

The two sets of equations (each given by Eqs. (2), (3),(6)–(9) for $T^{(1)}(x, y)$ and $T^{(2)}(x, y)$ are coupled using a finite difference equation for V_g:

$$V_g(x) = \frac{H^{(2)}(x) - H^{(1)}(x)}{\Delta t}, \tag{10}$$

where $H^{(j)}(x)$ is the vertical position of the interface as calculated by the QSS equations associated with time $t^{(j)}$ $(j = 1, 2)$. Thus, strictly speaking, the solution at time $t^{(1)}$ is obtained using a forward difference approximation for $V_g(x)$ while the solution for $t^{(2)}$ is based on a backward difference approximation for $V_g(x)$. The solution to the problem is finally defined as

$$T(x, y, t) = \frac{T^{(1)}(x, y) + T^{(2)}(x, y)}{2} \tag{11}$$

and

$$H(x, t) = \frac{H^{(1)}(x) + H^{(2)}(x)}{2}, \tag{12}$$

where $t = [t^{(1)} + t^{(2)}]/2$.

The Galerkin finite element method (GFEM) [12] with spine-parameterization [13] of the melt/crystal interface is applied to the MQSS problem. The temperature field, $T^{(1)}(x, y)$, is approximated by an expansion using two-dimensional bi-quadratic Lagrange basis functions associated with quadrilateral elements in a mesh conforming to the geometry of the solid and melt phases at time $t^{(1)}$. The same procedure is repeated for $T^{(2)}(x, y)$, though in this case the mesh is associated with the slightly different geometry of the phases at time $t^{(2)}$. The interface vertical positions $H^{(1)}(x)$ and $H^{(2)}(x)$ are expanded using one-dimensional quadratic Lagrange basis functions where, for convenience, the same horizontal distances between vertical spines (i.e. the same mesh spacing in the x-coordinate direction) is applied at $t^{(1)}$ and $t^{(2)}$. Next, Eqs. (7) and (9) are weighted and integrated in the usual manner (see e.g. Ref. [8]) using the temperature field, interface position, and mesh associated with time $t^{(1)}$. This method for generating Galerkin weighted residual equations is repeated for time $t^{(2)}$, and an additional set of residual equations is obtained by considering Eq. (10) at every finite element mesh node-point along the melt/crystal interface.

The above discretization process yields five coupled sets of nonlinear algebraic residual equations (for nodal values of $T^{(1)}(x, y)$, $T^{(2)}(x, y)$, $H^{(1)}(x)$, $H^{(2)}(x)$ and $V_g(x)$) which are solved using the Newton–Raphson technique. The finite time difference used for calculation of $V_g(x)$ (see

Eq. (10)) was chosen as $\Delta t = 1.2$ s; sample results were found not to be significantly affected by a factor of three reduction in this Δt value. Meshes used in the calculations presented here consist of 160 nine-node Lagrangian quadrilateral elements[2]. SQSS results shown in this manuscript are obtained with the same finite element (and associated mesh sizes), isotherm-method and Newton–Raphson techniques used for the MQSS problem. The transient equations (1)–(8) are also solved using a similar approach (with the same mesh sizes), where a backward-Euler fixed time-stepping technique is employed for discretization of temporal derivatives; an initial condition, which simulates a situation where growth starts from a stable melt/crystal interface position achieved within a stationary furnace temperature profile, is obtained by solving the SQSS problem with a zero furnace cooling rate ($G^{\star} = 0$). All the transient results presented were obtained using a time step of $\Delta t = 45$ s; select results were found not to change significantly when recalculated with $\Delta t = 15$ s.

2.2. One-dimensional analysis

It is often instructive (and efficient) to use one-dimensional analysis while studying systems of the type considered here, thus yielding an understanding of the (cross-sectional) area-averaged temperature field. The partial differential equation describing heat transport in the system is, in this case, given by

$$\rho_i C_{p_i} \frac{\partial T}{\partial t} = \frac{\partial}{\partial y}\left(k_i \frac{\partial T}{\partial y}\right) + 2\frac{h}{B}[T_{\mathrm{f}}(y,t) - T], \quad i = \mathrm{m},\ \mathrm{s}, \tag{13}$$

which together with appropriate boundary and initial conditions yields the time dependent one-dimensional temperature distribution in the melt and solid phases. When QSS analysis is justified and the MQSS approach is invoked, Eq. (13) and its boundary conditions are replaced by two ordinary differential equations:

$$\frac{\mathrm{d}}{\mathrm{d}y}\left(k_i \frac{\mathrm{d}T^{(j)}}{\mathrm{d}y}\right) + 2\frac{h}{B}[T_{\mathrm{f}}(y,t^{(j)}) - T^{(j)}] = 0, \quad i = \mathrm{m},\ \mathrm{s};\ j = 1,\ 2, \tag{14}$$

with two sets of boundary conditions

$$k_{\mathrm{s}} \frac{\mathrm{d}T^{(j)}}{\mathrm{d}y}\Big|_{y=0} = h[T^{(j)} - T_{\mathrm{C}}(t^{(j)})], \quad j = 1,\ 2, \tag{15}$$

$$-k_{\mathrm{m}} \frac{\mathrm{d}T^{(j)}}{\mathrm{d}y}\Big|_{y=L} = h[T^{(j)} - T_{\mathrm{H}}(t^{(j)})], \quad j = 1,\ 2, \tag{16}$$

the melt/crystal interface conditions

$$T^{(j)} = T_{\mathrm{mp}}, \quad j = 1,\ 2, \tag{17}$$

$$\left[-k_{\mathrm{m}}\left(\frac{\mathrm{d}T^{(j)}}{\mathrm{d}y}\right)_{\mathrm{m}} + k_s\left(\frac{\mathrm{d}T^{(j)}}{\mathrm{d}y}\right)_{\mathrm{s}}\right] = \Delta H_{\mathrm{f}} V_{\mathrm{g}}, \quad j = 1,\ 2, \tag{18}$$

and the one-dimensional version of the equation defining the growth velocity (Eq. (10)):

$$V_{\mathrm{g}} = \frac{H^{(2)} - H^{(1)}}{\Delta t}. \tag{19}$$

Substituting (for $j = 1$ and 2) the solution of Eq. (14) and associated boundary conditions (15)–(17) into Eq. (18), together with Eq. (19), yields a system of three nonlinear algebraic equations for dimensionless interface coordinates $z^{\star(1)} \equiv H^{(1)}/L$, $z^{\star(2)} \equiv H^{(2)}/L$ and interface velocity $V \equiv V_{\mathrm{g}}/V_{\mathrm{p}}$:

$$1 - K - SV + a_{\mathrm{s}}[A_{\mathrm{s}}^{(1)}\sinh(a_{\mathrm{s}} z^{\star(1)}) + C_{\mathrm{s}}^{(1)}\cosh(a_{\mathrm{s}} z^{\star(1)})] - Ka_{\mathrm{m}}[A_{\mathrm{m}}^{(1)}\sinh(a_{\mathrm{m}} z^{\star(1)}) + C_{\mathrm{m}}^{(1)}\cosh(a_{\mathrm{m}} z^{\star(1)})] = 0, \tag{20}$$

$$1 - K - SV + a_{\mathrm{s}}[A_{\mathrm{s}}^{(2)}\sinh(a_{\mathrm{s}} z^{\star(2)}) + C_{\mathrm{s}}^{(2)}\cosh(a_{\mathrm{s}} z^{\star(2)})] - Ka_{\mathrm{m}}[A_{\mathrm{m}}^{(2)}\sinh(a_{\mathrm{m}} z^{\star(2)}) + C_{\mathrm{m}}^{(2)}\cosh(a_{\mathrm{m}} z^{\star(2)})] = 0, \tag{21}$$

$$V = \frac{z^{\star(2)} - z^{\star(1)}}{\theta^{\star(2)} - \theta^{\star(1)}}, \tag{22}$$

where $a_{\mathrm{s}}, a_{\mathrm{m}}, A_{\mathrm{s}}^{(j)}, A_{\mathrm{m}}^{(j)}, C_{\mathrm{s}}^{(j)}, C_{\mathrm{m}}^{(j)}$ ($j = 1,\ 2$) are dimensionless expressions defined in the appendix, $K = k_{\mathrm{m}}/k_{\mathrm{s}}$, $S = \Delta H_{\mathrm{f}} V_{\mathrm{p}}/(k_{\mathrm{s}} G)$, and $\theta^{\star(j)} = \theta^{\star}(t^{(j)}) = [T_{\mathrm{mp}} - T_{\mathrm{C}}(t^{(j)})]/[T_{\mathrm{H}}(t^{(j)}) - T_{\mathrm{C}}(t^{(j)})]$ ($j = 1,\ 2$) is the melting point temperature rendered dimensionless using the (time dependent) cold-zone

[2] Taking advantage of symmetry, the discretized problem is solved on half the domain $0 < x < B/2$. In addition, select results were tested not to change significantly upon mesh refinement, where the refined mesh consists of 360 elements.

temperature and (time-independent) difference between hot-and-cold zone temperatures. Looking at this definition of $\theta^{\star}(t)$, together with Eqs. (4) and (5) and the fact that $T_{C_0} = T_{mp}$ (see Section 2.1), it can be shown that $\theta^{\star} = \tau$, where $\tau \equiv tV_p/L = tG^{\star}/(GL)$ is the dimensionless time evolved since the solidification process was initiated. More details on the derivation and solution of Eqs. (20)–(22) can be found in the appendix.

3. Results and discussion

The MQSS approach should, in theory, be valid in all situations where the QSS approximation is applicable. Here we test the new approach using the idealized system described above with properties taken from Ref. [14] and parameters loosely based on those in Ref. [10] (see Table 1); these were derived for a base-case analysis of a typical single component semiconductor material (e.g. silicon).

As a first step we present (in Fig. 2(a)) the dimensionless melt/crystal interface position at the centerline ($x = 0$), calculated for base-case parameter values using both transient and SQSS algorithms. In the case of the SQSS analysis, τ, the dimensionless time evolved since the solidification process was initiated, is calculated using its equivalence (derived from Eq. (3)) with the dimensionless position of the melting point temperature in the furnace, $\tau = tG^{\star}/(GL) = y_{f_{mp}}/L$. Here $y_{f_{mp}}$

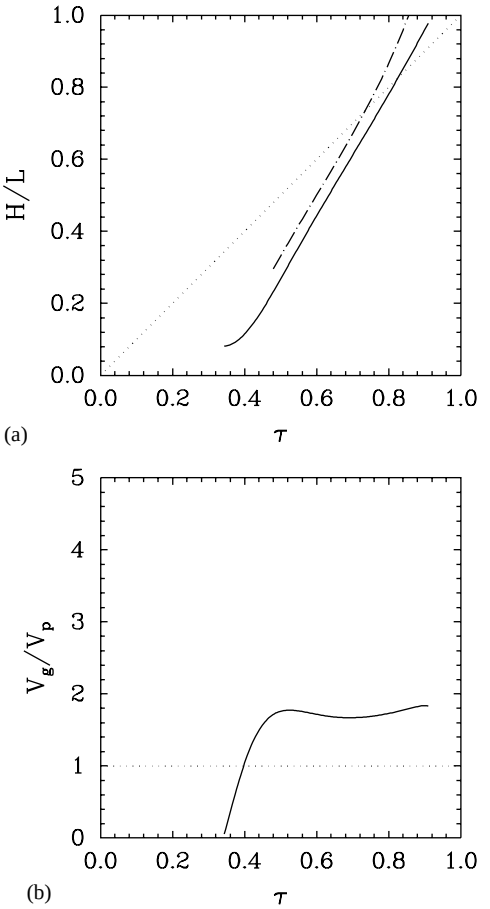

Fig. 2. Evolving melt/crystal interface position (a) and crystal growth velocity (b) along the centerline of the ampoule (base case). Solid line—transient calculation, dashed-dotted line—SQSS model, dotted line—steady-state case (for $L \to \infty$).

Table 1
Physical properties [14] and parameters (based on Ref. [10])

Description	Symbol	Base case value	Comment
Heat of fusion	ΔH_f	4122 J/cm^3	
Thermal conductivity of melt	k_m	0.54 W/cm K	Varied
Thermal conductivity of solid	k_s	0.22 W/cm K	Varied
Melting point	T_{mp}	1683 K	
Melt heat capacity	$\rho_m C_{p_m}$	2.53 J/cm^3 K	
Solid heat capacity	$\rho_s C_{p_s}$	2.29 J/cm^3 K	
Furnace cooling rate	$G^{\star}$	150 K/h	Varied
Furnace temperature gradient	G	50 K/cm	Varied
Ambient heat transfer coefficient	h	0.025 W/cm^2 K	Varied
Ampoule length (height)	L	10 cm	Varied
Ampoule width	B	2 cm	
Ampoule pull rate	$V_p = G^{\star}/G$	3 cm/h	Varied

is the vertical (y) coordinate position in the furnace at which its temperature is T_{mp}.

The ratio of characteristic time scales associated with the example ($\tau_g/\tau_t = 288$) justifies invoking the QSS approximation. However, judging by the results shown in Fig. 2(a) this assumption, applied using the SQSS approach, grossly overestimates the vertical position of the interface in the ampoule. This inaccuracy can be directly related to the rate of latent heat release which, in the case of the SQSS approach is estimated to be 40% lower than the correct rate predicted by the transient analysis (see Fig. 2(b); note that the rate of latent heat release is directly proportional to the growth rate). Thus, this practical example demonstrates that assuming $V_p = V_g$ (i.e. using the SQSS method) may lead to significant inaccuracies in the analysis despite the validity of the QSS assumption.

The significant difference (in Fig. 2) between the predicted centerline positions of the melt/crystal interface is attributed to the incorrect assumption, used in the SQSS analysis, that $V_g = V_p$. In Fig. 3 the results shown in Fig. 2 are replotted together with those obtained using the MQSS approach. It is evident that, contrary to the SQSS calculation, the MQSS method yields a predicted centerline interface position which is in very good agreement with that obtained using the transient analysis. Looking at Fig. 3(b) it can be concluded that this agreement is due to the successful prediction of the growth velocity by the MQSS analysis for intermediate and late stages of the growth process. The discrepancy between the results, during the initial stages of growth, is most probably due to the initial transient. Notice that the initial condition, which results in $V_g(t = 0) = 0$, is imposed only in the transient calculation since it is not required when using the MQSS approach. Finally, an additional set of results shown in Fig. 3 and obtained using the 1-D semi-analytical MQSS model, serves as a benchmark for our 2-D numerical calculation as well as demonstrates the applicability of a 1-D approximation for the case depicted in this figure.

The success of applying the MQSS approach to the two-dimensional base-case problem associated with Figs. 2 and 3 is further demonstrated by

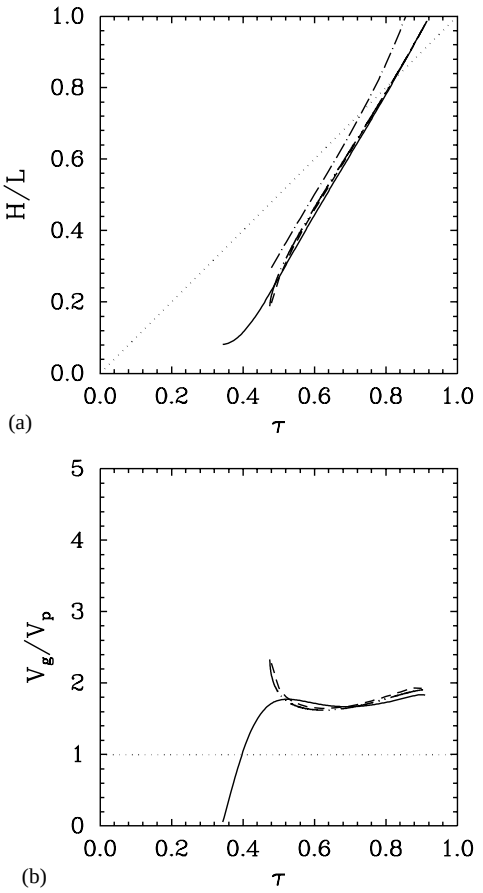

Fig. 3. Results presented in Fig. 2 supplemented with two-dimensional (dashed lines) and one-dimensional (dash-dot-dot lines) MQSS calculations.

observing the melt/crystal interface position and growth profiles (i.e. $H(x)$, $V_g(x)$) at a specific time during the growth process; these are depicted in Fig. 4 for $\tau = \theta^{\star} = 0.79$. Although the dependence of V_g on position (x) is weak, it can be seen that it is fairly well captured by the MQSS calculation. In addition, in this case it can be seen that the sign of interface curvature is correctly predicted by the MQSS calculation and *incorrectly* predicted using the SQSS approach. This special situation, due to the inherent change in sign of interface curvature at $H(x) \approx 8$ cm, demonstrates the potential for qualitative inaccuracies when using the SQSS method.

Within the framework of QSS analysis, the growth rate affects evolving thermal fields through

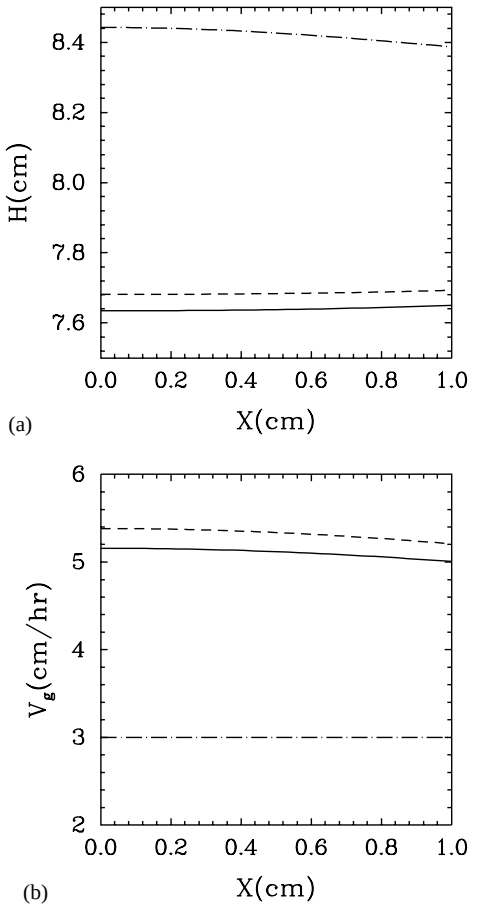

Fig. 4. Interface shapes (a) and crystal growth velocity profiles (b) calculated using different methods (base case). Solid lines—transient calculation, dashed lines—MQSS model, dashed-dotted lines—SQSS approach.

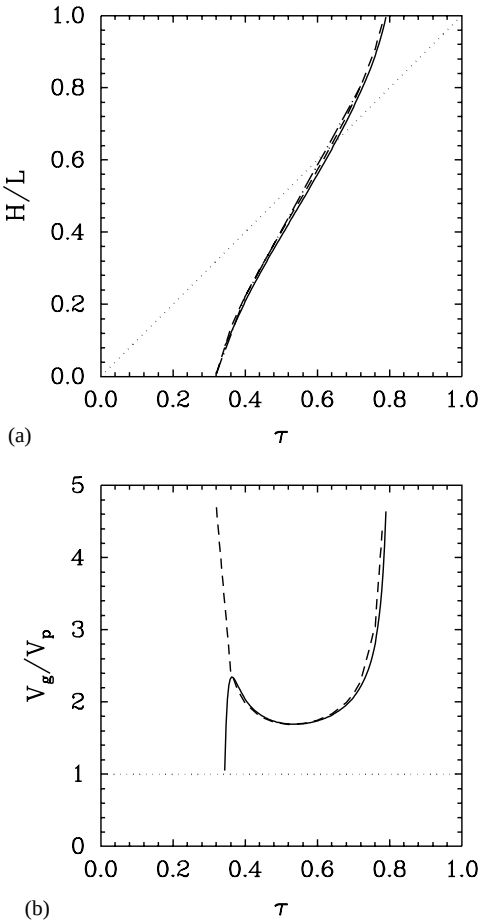

Fig. 5. Evolving melt/crystal interface position (a) and crystal growth velocity (b) along the centerline of the ampoule ($\Delta H_f = 0$). Solid line—transient calculation, dashed line—MQSS model, dashed-dotted line—SQSS approach, dotted line—steady-state solution (for $L \to \infty$).

a single term in the model equations. In the event that latent heat of solidification is negligible, this term (right-hand side of Eq. (6)) is rendered unimportant and the value of V_g should have no effect on the evolving thermal field. In Fig. 5(a), the centerline interface position, as a function of time, is plotted for the case of $\Delta H_f = 0$. Excellent agreement is observed between SQSS, MQSS and transient analysis results. This is consistent with the idea that the value of V_g is unimportant in this case, as well as with the assumption that QSS analysis is valid for the system studied in this manuscript. When the QSS approach is justified, sensible heat effects are mostly unimportant and the difference between transient, SQSS and MQSS results can be largely attributed to inaccuracies in estimates of V_g which are manifested through latent heat effects. In the special case depicted in Fig. 5(a), both sensible and latent heat effects are unimportant and therefore all three calculations produce similar results. Finally, notice that the growth rate, which is in this case very different from the pull rate (see Fig. 5(b)), is quite accurately calculated using the MQSS approach except during a very short initial time-period.

Unlike QSS analyses of directional crystal growth, steady-state simulations [15–18] are restricted to infinitely long systems and are characterized by the equality $V_g = V_p$. It is therefore expected and observed (see Fig. 6 as compared with Fig. 3) that as the ampoule length (L) is increased, the growth velocity should approach that of the steady-state limit ($V_g(x)/V_p \to 1.0$). Our calculations (not shown here) indicate that this limit is also approached when h is significantly increased. In this case, of large h values, one would expect the surface temperature field ($T(x = \pm B/2, y)$) to approach furnace profile values thereby resulting in $V_g(x = \pm B/2) \to V_p$;

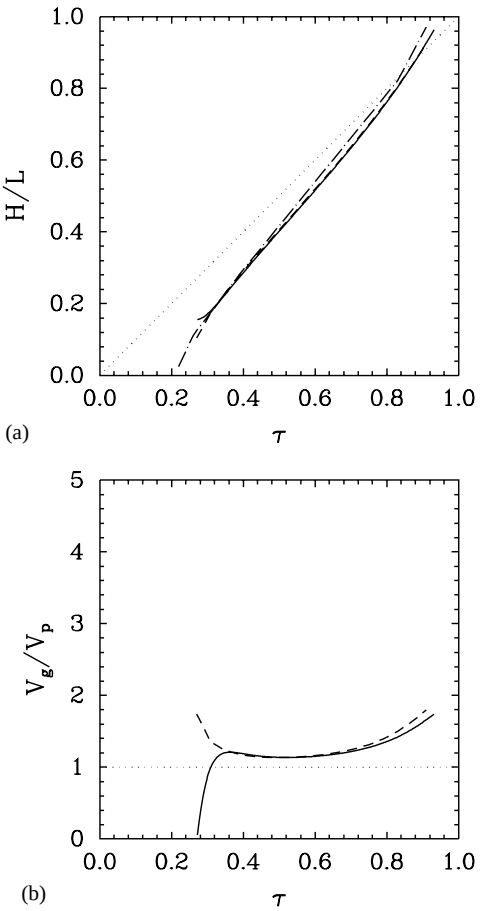

Fig. 6. Evolving melt/crystal interface position (a) and crystal growth velocity (b) along the centerline of the ampoule ($L = 20$ cm). Solid lines—transient calculation, dashed lines—MQSS model, dashed-dotted line—SQSS approach, dotted line—steady-state solution (for $L \to \infty$).

this should logically result in a stronger "enforcement" of the induced growth rate (V_p) for all values of x. Consistent with these observations, it can be shown that using the SQSS approach becomes a reasonable option for relatively long ampoules (see Fig. 6) and relatively large h values.

When applying QSS analysis the only material properties of importance are the volumetric latent heat of solidification (ΔH_f) and the thermal conductivities of melt (k_m) and solid (k_s). The effect of ΔH_f on results from SQSS and MQSS analyses are discussed above. The values of k_s and k_m are first and foremost important in the determination of the validity of the QSS approach via their impact on τ_g/τ_t (see Section 1). As implied above, all k_s, k_m values used here are consistent with a valid QSS analysis. In Fig. 7, we present results obtained with an increased solid phase thermal conductivity; the melt thermal conductivity is kept at its base-case value (see Table 1). As can be seen in this figure, raising the value of solid-phase thermal conductivity leads to an increase in the deviation between centerline interface positions predicted by the SQSS technique and those calculated using the transient analysis. This can be directly attributed to an increase in the difference between V_g and V_p (Fig. 7(b)). Applying the modified (MQSS) approach in this case, results in a good prediction of V_g and an excellent agreement between centerline interface positions calculated using this technique and those obtained with the transient analysis. Finally, when reducing k_s and k_m below the base case values (see Fig. 8), very good agreement is found between the SQSS, MQSS and transient calculations of centerline interface positions. This is most probably a consequence of a better agreement (compared to the base case) between V_g and V_p values in this case.

The effect of thermal conductivity on the agreement between V_g and V_p (and therefore on the validity of the SQSS approach) can be understood through the definition of the dimensionless heat transfer coefficient, the Biot number $Bi_i = hB/(2k_i)$, $i = m, s$. Here lowering the value of thermal conductivity effectively increases the value of the dimensionless heat transfer coefficient; increasing the value of thermal conductivity has an opposite effect on the Biot number. It is therefore understandable that trends associated

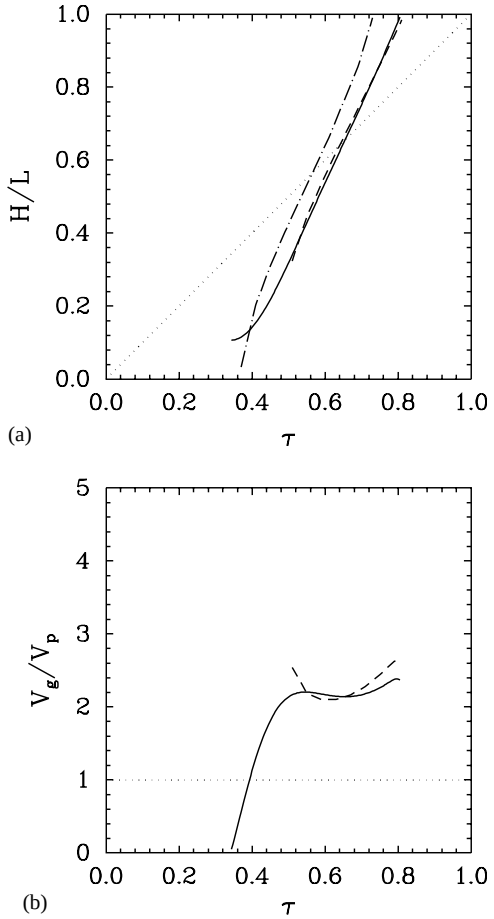

Fig. 7. Evolving melt/crystal interface position (a) and crystal growth velocity (b) along the centerline of the ampoule ($k_m = k_s = 0.54\,W/cm\,K$). Solid lines—transient calculation, dashed lines—MQSS model, dashed-dotted line—SQSS approach, dotted line—steady-state solution (for $L \to \infty$).

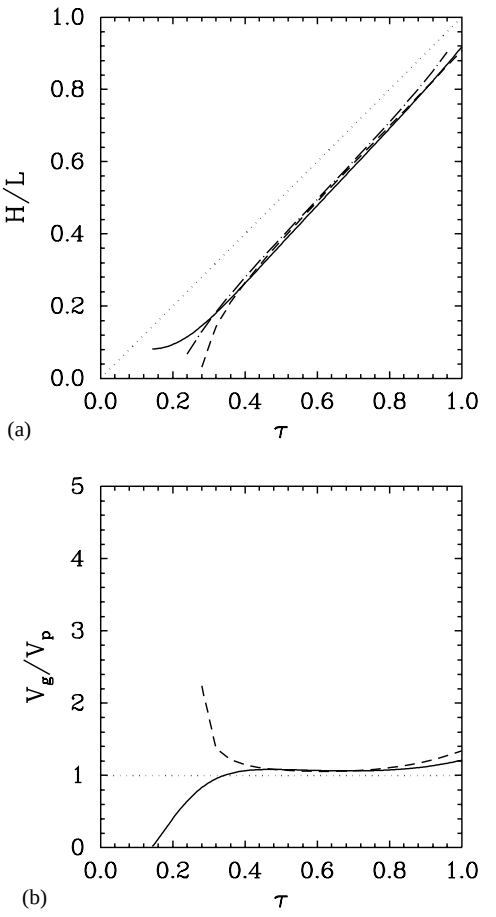

Fig. 8. Evolving melt/crystal interface position (a) and crystal growth velocity (b) along the centerline of the ampoule ($k_m = k_s = 0.055\,W/cm\,K$). Solid lines—transient calculation, dashed lines—MQSS model, dashed-dotted line—SQSS approach, dotted line—steady-state solution (for $L \to \infty$).

with decreasing the thermal conductivity are observed to be the same as those caused by increasing the value of h and vice versa. The impact of k_s on the value of V_g is not, however, confined to the effect of the Biot number on the results. Looking at the definition of S (see Section 2.2), decreasing the value of k_s corresponds to increasing the value of ΔH_f and should have a similar effect on the results. Comparing Fig. 3(b) ($S = 0.31$) and Fig. 5(b) ($S = 0$), while ignoring the initial transients, it is interesting to note that the minimum value of $V_g(x)$ is almost the same in both these figures ($V_g/V_p \approx 1.7$). This, together with a comparison of Fig. 7(b) ($S = 0.127$) with Figs. 3(b) and 5(b) (again, ignoring initial transients), suggests that the effect of k_s on the minimum value of V_g (and therefore, to a large extent, on the validity of the SQSS approach) is dominated by its impact on the Biot number.

4. Conclusions

The QSS approach to modeling heat transfer during directional crystal growth is valid as long as relevant transport mechanisms are fast compared

with the growth rate. However, applying QSS analysis when investigating these systems is problematic since the growth rate, which is required for the analysis, is not known a priori. The MQSS method proposed here allows for the determination of thermal fields in the system using a self-consistent approach which uses the calculated growth rate when accounting for latent heat effects.

The MQSS analysis method is applied to an idealized VGF system, employed in the directional growth of a prototype single component semiconductor material. Results demonstrate the superiority of this approach as compared to the SQSS method which uses the assumption of $V_p = V_g$. Centerline interface positions calculated using the MQSS technique show excellent agreement with those calculated using a rigorous transient solution scheme. In addition, a select base-case solution is shown to agree with that of a one-dimensional semi-analytical version of the MQSS method thereby confirming the reliability of the two-dimensional formulation.

The excellent agreement between results of the MQSS analysis and that of the transient calculation, observed for all parameters considered in this manuscript, stands in contrast to deviations between SQSS predictions and those of the transient analysis. The failure of the SQSS approach is strongly linked to the significant rate of latent heat release considered here ($S = 0.31$) together with deviations of V_g from V_p. The SQSS method is, however, successful in situations where latent heat release is negligible ($S \ll 1$) or in cases where V_g approaches V_p. As shown and discussed in Section 3, the latter situation ($V_g = V_p$) is approached when the ampoule length is increased, the convective heat transfer coefficient is large in magnitude and the charge thermal conductivity is reduced. These observations are qualitatively consistent with trends expected when looking at the criterion suggested by Sukanek [3]. This criterion, which was developed for a Bridgman–Stockbarger system, is based on several calculations involving a range of parameter values. Therefore, despite the non-trivial differences between the VGF system studied here and the Bridgman–Stockbarger furnace analyzed in Ref. [2,3], it is interesting to quantitatively test the applicability of Sukanek's criterion with respect to the results presented in Figs. 2–8. Following Sukanek [3], and ignoring differences in geometry of ampoule (slab versus cylinder) and furnace temperature profile (uniform gradient versus the hot-adiabatic-cold zones), less than 10% deviation between V_g and V_p should be obtained in over 70% of the ampoule when

$$L \geqslant 7.07\sqrt{kB/(2h)}, \tag{23}$$

where to be conservative, we choose k to be the maximum between melt and solid conductivity values. According to Eq. (23), the minimum ampoule lengths needed to satisfy this criterion are, 33 cm for results presented in Figs. 2–7 and 10 cm for the results shown in Fig. 8. Parameter values used to obtain Figs. 2–7 therefore violate Sukanek's criterion; this is consistent with the relatively large values of V_g/V_p shown in these figures. On the other hand, parameters associated with the results shown in Fig. 8 yield (via Eq. (23)) a minimum ampoule length which is the same as the value of L used here ($L = 10$ cm) thereby satisfying Sukanek's criterion. It is remarkable to observe, that despite the differences between the VGF system and the system considered by Sukanek, semi-quantitative agreement is achieved between the level of deviation (between V_g and V_p) that should occur in this case, according to Sukanek, and the actual values of $V_g(x)/V_p$ shown in Fig. 8(b).

Applying the MQSS approach is not without penalty. The simultaneous solution of two coupled sets of QSS equations results in slightly over a factor of two increase in the number of unknowns. Assuming Gauss Elimination is applied in the solution of the linear system, this translates into anything between a factor two to a factor of eight increase in computational costs, depending on the structure of the system of equations [19]. However, it is our belief that the level of added accuracy offered by the MQSS approach makes this added computational expense worthwhile. If, however, computational resources are limited, it is still possible in some cases to justify using the SQSS method based on assessments of the rate of latent heat release (S) and of Sukanek's criterion [3]. Finally, it should be stressed that both the SQSS

and MQSS methods are prone to failure during initial stages of growth. This is not surprising; the QSS approach is not recommended during the initial transient.

Acknowledgment

AV acknowledges partial support by the Israel Absorption Ministry.

Appendix A

Solving Eqs. (14) with boundary conditions (15)–(17) (without, at this stage, the Stephan condition and growth velocity equation Eqs. (18) and (19) yields algebraic relations for temperatures and interface positions. Using dimensionless temperatures $\theta^{(j)} = [T^{(j)} - T_C(t^{(j)})]/[T_H(t^{(j)}) - T_C(t^{(j)})]$, the vertical coordinate $z = y/L$, interface positions $z^{\bigstar(j)} = H^{(j)}/L$ and parameters $Bi_i = hB/(2k_i)$, $\Lambda = 2L/B$, $a_i = \Lambda\sqrt{Bi_i}$, $\theta^{\bigstar(j)} = [T_{mp} - T_C(t^{(j)})]/[T_H(t^{(j)}) - T_C(t^{(j)})]$ $(i = m,\ s;\ j = 1, 2)$, these relations may be written in the form

$$\theta^{(j)} = A_i^{(j)}\cosh(a_i z) + C_i^{(j)}\sinh(a_i z) + z, \quad i = m, s;\ j = 1, 2, \tag{A.1}$$

where

$$A_s^{(j)} = \frac{a_s(\theta^{\bigstar(j)} - z^{\bigstar(j)}) + \sinh(a_s z^{\bigstar(j)})}{a_s\cosh(a_s z^{\bigstar(j)}) + \Lambda Bi_s\sinh(a_s z^{\bigstar(j)})}, \tag{A.2}$$

$$C_s^{(j)} = \frac{\Lambda Bi_s(\theta^{\bigstar(j)} - z^{\bigstar(j)}) - \cosh(a_s z^{\bigstar(j)})}{a_s\cosh(a_s z^{\bigstar(j)}) + \Lambda Bi_s\sinh(a_s z^{\bigstar(j)})}, \tag{A.3}$$

$$A_m^{(j)} = \frac{(\theta^{\bigstar(j)} - z^{\bigstar(j)})[\Lambda Bi_m\sinh(a_m) + a_m\cosh(a_m)] + \sinh(a_m z^{\bigstar(j)})}{D^{(j)}}, \tag{A.4}$$

$$C_m^{(j)} = -\frac{(\theta^{\bigstar(j)} - z^{\bigstar(j)})[\Lambda Bi_m\cosh(a_m) + a_m\sinh(a_m)] + \cosh(a_m z^{\bigstar(j)})}{D^{(j)}}, \tag{A.5}$$

and

$$D^{(j)} = \cosh(a_m z^{\bigstar(j)})[\Lambda Bi_m\sinh(a_m) + a_m\cosh(a_m)] - \sinh(a_m z^{\bigstar(j)})[\Lambda Bi_m\cosh(a_m) + a_m\sinh(a_m)]. \tag{A.6}$$

Substituting (A.1) in dimensionless versions of (18) and (19) leads to the system of three nonlinear algebraic equations (Eqs. (20)–(22)) given in Section 2.2. These three nonlinear algebraic equations were solved (for the unknowns V, $z^{\bigstar(1)}$, $z^{\bigstar(2)}$) using a standard Newton–Raphson technique. As in the case of 2-D analysis (see Section 2.1), the solution at time $t = [t^{(1)} + t^{(2)}]/2$ is defined as $T(y, t) = [T^{(1)}(y) + T^{(2)}(y)]/2$ and $H(t) = [H^{(1)} + H^{(2)}]/2$. Finally, note that $\theta^{\bigstar(2)} - \theta^{\bigstar(1)} = \Delta\tau$ values ranged between 5×10^{-4} and 9×10^{-4} in the calculations shown here. Select results were found not to change significantly upon an order of magnitude reduction in these $\Delta\tau$ values.

References

[1] F. Dupret, N. Van Den Bogaert, in: D.T.J. Hurle (Ed.), Handbook of Crystal Growth, Vol. 2b: Bulk Crystal Growth, Growth Mechanisms and Dynamics, North-Holland, Amsterdam, 1994, p. 875.
[2] P.C. Sukanek, J. Crystal Growth 58 (1982) 208.
[3] P.C. Sukanek, J. Crystal Growth 58 (1982) 219.
[4] T.W. Clyne, J. Crystal Growth 50 (1980) 684.
[5] T.W. Clyne, J. Crystal Growth 50 (1980) 691.
[6] J.J. Derby, R.A. Brown, J. Crystal Growth 87 (1988) 251.
[7] S. Kuppurao, J.J. Derby, J. Crystal Growth 172 (1997) 350.
[8] S. Brandon, D. Gazit, A. Horowitz, J. Crystal Growth 167 (1996) 190.
[9] Y. Liu, A. Virozub, S. Brandon, J. Crystal Growth 205 (1999) 333.
[10] C.A. Wang, A.F. Witt, J.R. Carruthers, J. Crystal Growth 66 (1984) 299.
[11] S. Brandon unpublished results.
[12] G. Strang, G.J. Fix, An Analysis of the Finite Element Method, Prentice–Hall, Englewood Cliffs, NJ, 1973.
[13] B.A. Finlayson, Numerical Methods for Problems with Moving Fronts, Ravenna Park Publishing, Inc., Seattle, 1992.
[14] Kyung-Woo Yi, Hyung-Tae Chung, Hong-Woo Lee, Jong-Kyu Yoon, J. Crystal Growth 132 (1993) 451.
[15] C.E. Chang, W.R. Wilcox, J. Crystal Growth 21 (1974) 135.
[16] T.-F. Fu, W.R. Wilcox, J. Crystal Growth 48 (1980) 416.
[17] R.J. Naumann, J. Crystal Growth 58 (1982) 554.
[18] R.J. Naumann, J. Crystal Growth 58 (1982) 569.
[19] G. Dahlquist, Å. Björck, Numerical Methods, Prentice–Hall, Englewood Cliffs, NJ, 1974.